Photophysical oxidation of HCHO produces HO2 radicals

Blair Welsh, Maggie Corrigan, Emmanuel Assaf, Klaas Nauta, Paolo Sebastianelli, Meredith Jordan, Christa Fittschen, Scott Kable

Sunlight-driven combustion of HCHO in the troposphere: Photophysical Oxidation of HCHO produces HO_2 radicals

Blair Welsh,[1,†] Maggie Corrigan,[2] Emmanuel Assaf,[3,‡] Klaas Nauta,[1] Paolo Sebastianelli,[1]

Meredith J. T. Jordan,[2] Christa Fittschen[3] and Scott H. Kable[1*]

[1] School of Chemistry, University of New South Wales, Kensington, NSW, 2052, Australia.

[2] School of Chemistry, University of Sydney, Sydney, NSW, 2006, Australia.

[3] Université Lille, CNRS, UMR 8522 - PC2A - Physicochimie des Processus de Combustion et de l'Atmosphère, F-59000 Lille, France.

*Corresponding author. Email: s.kable@unsw.edu.au

[†] Present address: Combustion Research Facility, Sandia National Laboratories, Livermore, California, 94551, USA

[‡] Present address: Chemical Sciences Laboratory, National Oceanic and Atmospheric Administration, 325 Broadway, Boulder, CO 80305 USA and Cooperative Institute for Research in Environmental Sciences, University of Colorado, Boulder, CO, USA

Abstract

Formaldehyde, HCHO, is the highest volume carbonyl in the atmosphere. After absorption of sunlight at wavelengths shorter than 330 nm it dissociates to form H and HCO radicals, which react with O_2 to form HO_2. In this paper, we report direct experimental detection of HO_2 radicals by cavity ringdown spectroscopy following photolysis of HCHO at photon energies *below* the energetic threshold for radical formation. At these same photon energies, end-product analysis by Fourier-transform infrared spectroscopy reveals indirectly the formation of HO_2 at 1 Bar pressure through the detection of formic acid, a product from secondary HO_2 reactions with the parent HCHO. Supported by electronic structure theory and master equation calculations, we attribute this to *photophysical oxidation* (PPO): photo-excited HCHO relaxes non-radiatively to the ground electronic state where the vibrationally activated molecules react with O_2. Thus PPO occurs under far-from-equilibrium conditions: the HCHO vibrational energy is close to the absorbed photon energy, whereas other degrees of freedom are thermalised. Radical formation via PPO has the opposite pressure dependence to photolysis – increasing for higher pressure of O_2. PPO is likely to be a general mechanism in tropospheric chemistry.

Introduction

Sunlight drives the chemistry of the atmosphere. Near the Earth's surface, absorption of light by molecules such as carbonyls produces highly reactive radical species. These radicals rapidly react with atmospheric oxygen in what is commonly described as photochemical oxidation (PCO), *i.e.* photolysis followed by oxidation. The resulting atmospheric HO_2 and OH radicals then initiate further radical chain reactions that cleanse the atmosphere of most pollutants and oxidise atmospheric carbon to CO_2 (*1*,*2*).

In the atmosphere, a gas phase molecule has four principal fates. It can *i)* absorb light and photolyse, or *ii)* react with a highly reactive species such as OH, NO_3 or O_3, or *iii)* undergo wet or dry deposition, or *iv)* the molecule might be long-lived, and hence globally distributed throughout the atmosphere. In this paper, we propose that *i)* and *ii)* combine in a new process where photo-activated molecules formed after a radiationless transition (a photophysical process) react with O_2 in a reaction that is similar to combustion, but under far-from-equilibrium conditions.

The reaction of activated (internally-excited) molecules is well-known. The products of exothermic reactions can be formed with an inverted distribution of energy in internal vibrational states. These chemically-activated molecules may react faster than those at thermal energies. For example, in an atmospheric context, Glowacki *et al* have shown that the chemically-activated hydroxyvinyl radical (HC=CHOH), formed from the reaction of OH with ethyne (HCCH), undergoes a different atmospheric fate depending on the degree of internal activation (*3*). Vibrational activation can also be achieved by infrared (IR) overtone excitation as discussed in an atmospheric context by Vaida and Donaldson (*4*). Such IR-induced activation in molecules such as H_2SO_4 can explain the SO_2 vertical profiles in the polar stratosphere. The enhanced reaction of electronically-activated species in the atmosphere is also well-known. Oxygen atoms in their excited ^1D electronic state react facilely with important atmospheric molecules, such as H_2O and N_2O, whereas ground state O(^3P) atoms are unreactive (*5*).

In this paper we demonstrate a different type of activated chemistry in formaldehyde (HCHO), and show that it is relevant under tropospheric conditions. The process is shown in Figure 1. A UV photon excites HCHO to its first excited singlet state, S_1. Internal conversion (IC) transfers the energy to the ground electronic state, S_0. As a photophysical process, energy is conserved and the energy of the excited electronic state is transferred to vibrational energy in the ground electronic

state. The photophysically-activated molecule then reacts with O_2 to initiate photophysical oxidation (PPO), forming HCO and HO_2 radicals. In the case of HCHO, the critical threshold energy for PPO (161 kJ mol^{-1}, (*6*)) is less than half of that required for PCO via radical formation from direct photolysis of the C-H bond (362.8 kJ mol^{-1}).

5

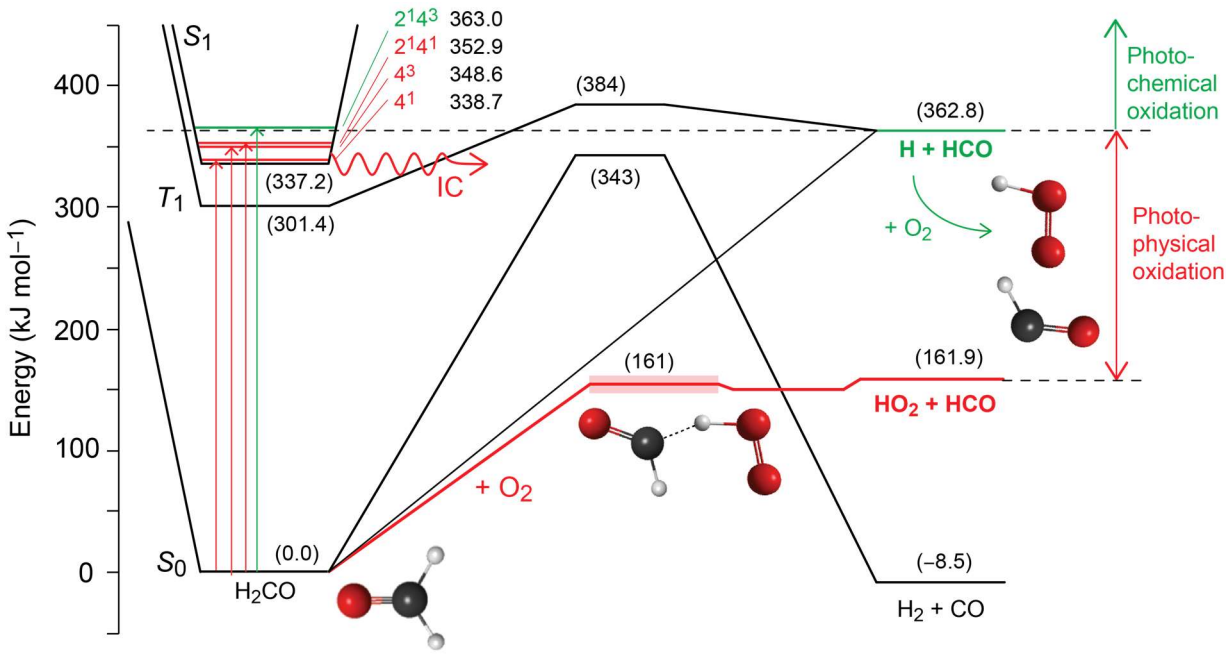

Fig. 1. Formaldehyde energy level diagram showing accessible photochemical (PCO) and photophysical oxidation (PPO) pathways following excitation to the indicated S_1 levels. The PCO pathway, via photolysis of the CH bond, is shown in green. PPO (red) occurs with a much lower threshold energy.

Like other activated chemical processes, PPO is a *far-from-thermal-equilibrium* mechanism. The reactive degrees of freedom in HCHO (vibration, rotation and translation) are not in equilibrium with each other, nor with the background gas. Consequently, PPO reactions will not behave with a conventional temperature and pressure dependence. Indeed, we predict PPO reactions in the troposphere will produce different chemical products, and have a reverse pressure dependence to conventional PCO, resulting in, as yet, unknown effects on tropospheric cycles. We predict PPO is a general mechanism for molecules that absorb light and conclude this paper by considering the implications that PPO might have for chemical models of the troposphere.

Formaldehyde (HCHO) is the simplest carbonyl and one of the most important organic species in the atmosphere. It is both directly emitted, and formed as an oxidation product of volatile organic species. Formaldehyde absorbs light in the near-ultraviolet spectrum ($\lambda \gtrsim 300$ nm at the Earth's surface), initiating several well-characterised photochemical processes (*7-13*). As a small molecule, HCHO is also a benchmark for high-level *ab initio* theory (*14-17*). The depth of knowledge about HCHO photochemistry – in the laboratory, in the atmosphere and theoretically – makes it an ideal candidate to demonstrate, unequivocally, the presence of the PPO reaction.

The spectroscopy, photochemistry and energetics of HCHO, applicable to this work, are described in detail in the supplementary information. Figure 1 shows a schematic of the relevant electronic states, energy levels and chemical pathways following near-UV excitation. When excited above the radical threshold ($\lambda < 330$ nm), HCHO has two photolysis outcomes:

$$\mathrm{HCHO} + h\nu \rightarrow \bullet\mathrm{HCO} + \mathrm{H}\bullet \qquad \text{(R1)}$$

and

$$\mathrm{HCHO} + h\nu \rightarrow \mathrm{H_2} + \mathrm{CO} \qquad \text{(R2)}$$

with threshold energies shown in Fig. 1. The total HCHO photolysis quantum yield (QY), ϕ_{ph}, for $\lambda < 330$ nm is essentially unity and largely pressure independent (*18-25*). In the troposphere, the radical products from R1 react quickly with O_2 to produce HO_2:

$$\mathrm{H}\bullet + \mathrm{O_2} \xrightarrow{\mathrm{M}} \mathrm{HO_2}\bullet \qquad \text{(R3)}$$

and

$$\bullet\mathrm{HCO} + \mathrm{O_2} \rightarrow \mathrm{HO_2}\bullet + \mathrm{CO} \qquad \text{(R4)}$$

where M is a collision partner needed to stabilise HO_2. The three reactions, R1, R3 and R4, together with the reaction of HCHO with OH and Cl atoms, constitute the main oxidation

pathways of HCHO (*26*). The conventional PCO of HCHO, R1 followed by R3 and R4, can only occur at absolute energies above the R1 radical threshold, which is known accurately to be 362.80 kJ mol^{-1} (*27*). Photon energies lower than this threshold can cause PCO if thermally excited HCHO molecules absorb light. Care is taken in this work not to excite vibrational hot-bands (see below).

At lower excitation energy (corresponding to longer wavelengths, $\lambda > 330$ nm), only the molecular photolysis channel, R2, is possible, and tunnelling allows R2 to proceed at energies below the classical energetic threshold shown in Fig. 1. Under tropospheric conditions, ϕ_{ph} is less than unity and pressure dependent (*18-22*); there is competition between R2 and collisions with (mainly) N_2 and O_2, which remove excess vibrational energy and return HCHO to thermal equilibrium. Here, we demonstrate that these collisions with O_2 can also lead to PPO of HCHO:

$$HCHO^{\ddagger} + O_2 \rightarrow \bullet HCO + HO_2 \bullet \qquad \text{(R5)}$$

where the double dagger represents vibrationally-activated HCHO.

Results

We employed two experimental techniques, with interpretation supported by *ab initio* electronic structure theory calculations of the critical energies of R5 and Master Equation kinetic modelling of PPO under experimental conditions. In both experiments, a laser was used to excite specific vibrational levels of the S_1 electronic state of HCHO as indicated in Fig. 1. Laser excitation, coupled with the well-known spectroscopy of HCHO (see Supplementary Information, SI), ensure that the initial, photoexcited energy of HCHO is very well-defined. The lower-lying excited levels, 4^1, 4^3 and $2^1 4^1$ lie 24, 14 and 10 kJ/mol below the radical threshold, respectively, while the higher lying level, $2^1 4^3$, is 0.2 kJ mol^{-1} above the radical threshold. The 4^1 level lies below the R2 energetic barrier to molecular products, however tunnelling through the barrier is efficient at this energy and molecular products are still observed, even in the presence of collisions at 1 Bar pressure (*11, 21*).

In the first experiment, cavity ring down spectroscopy (CRDS) was used in a low-pressure flow cell to measure *in situ* production of HO_2, following HCHO irradiation in the presence of O_2. In

the second experiment, Fourier-transform infrared (FTIR) spectroscopy was used to measure end-products following irradiation of HCHO in a static cell as a function of pressure. The CRDS experiments demonstrate unequivocal production of HO_2 radicals, but at a maximum pressure of 50 Torr. The FTIR experiments implicitly demonstrate PPO is operative at 1 Bar pressure. Further experimental details are provided in References *28* and *29* and in the Methods section (see SI).

Direct CRDS detection of HO_2: Figure 2 shows a CRDS action spectrum, where HO_2 absorption is plotted as a continuous function of photolysis wavelength. The complexities in the spectrum arise from the vibration-rotation structure of the HCHO electronic spectrum, which is well known (*30*, *31*). The spectrum can be simulated and assigned, as shown in the higher resolution inset panels. Above the radical threshold, transitions are very intense due to efficient PCO production of HO_2 via R3 and R4. The inset panels also have clearly assigned HCHO structure, shown in red, where

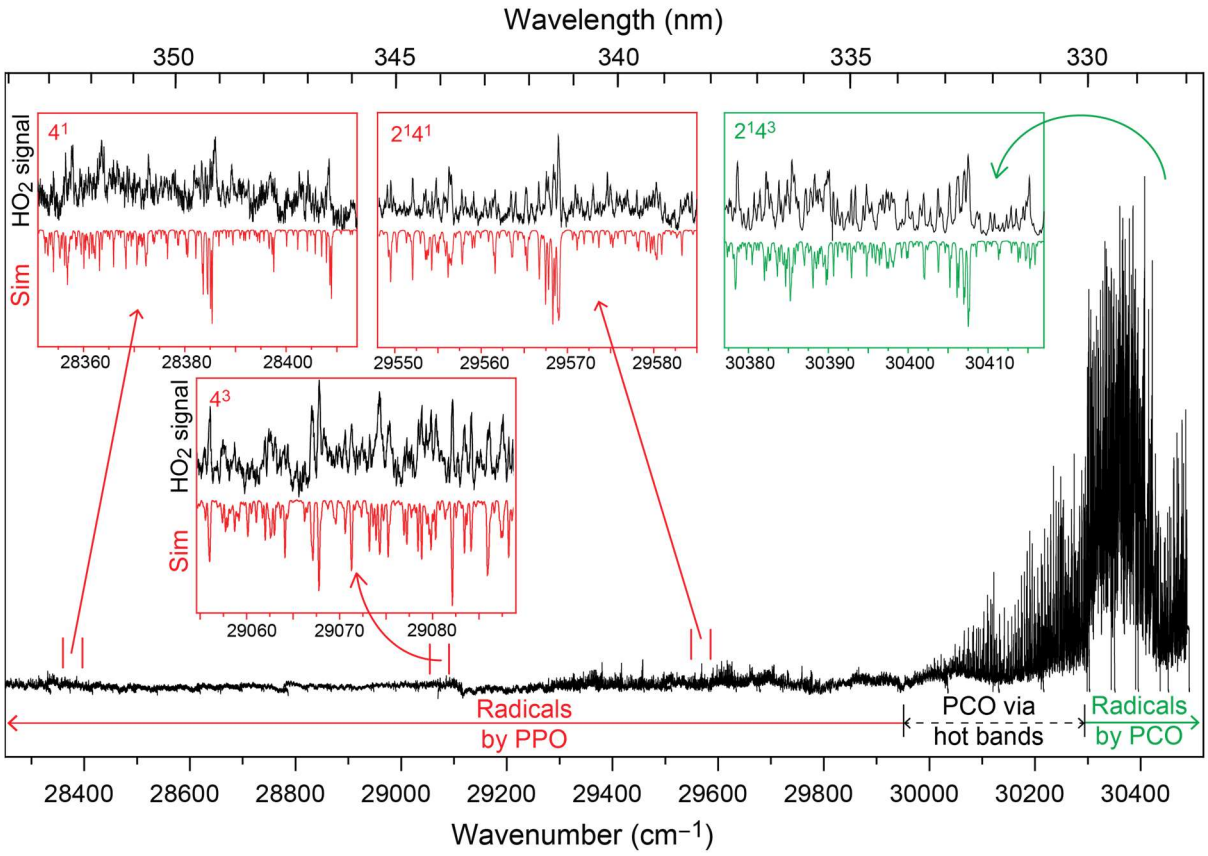

Fig. 2. Action spectrum of HCHO measured by CRDS of the HO_2 radical. HO_2 signal is found throughout the spectral range as shown by the simulated HCHO absorption spectra shown in each inset with expanded resolution. PCO is shown in green while PPO is shown in red. The upper wavelength axis is non-linear.

PCO production of HO_2 is not energetically possible. This is the region of photophysical production of HO_2. The signal-to-noise ratio for excitation to the 4^3 and, especially, 4^1 levels is

lower than $2^1 4^1$ in the PPO region because the absorption strength of these bands is ~1/3 that of $2^1 4^1$, and the laser energy is lower near 4^1. As shown below, the PPO quantum yield, however, is similar.

The dependence of the HO_2 signal on O_2 pressure at a total pressure of 50 Torr (balance helium) is shown in Fig. 3. The HO_2 signal below the radical threshold ($2^1 4^1$) shows a strong, linear increase with P(added O_2). The continued observation of radicals, and their linear increase with O_2 pressure are key observations of this work and indicate a new bimolecular chemical mechanism for radical formation.

The HO_2 signal above the radical threshold ($2^1 4^3$) shows a small increase with increasing O_2 pressure. The observed HO_2 at P(added O_2) = 0 is due to background O_2, which we estimate from the measured leak rate as ~10^{14} cm^{-3} (3 mTorr). Because the background O_2 is about four orders

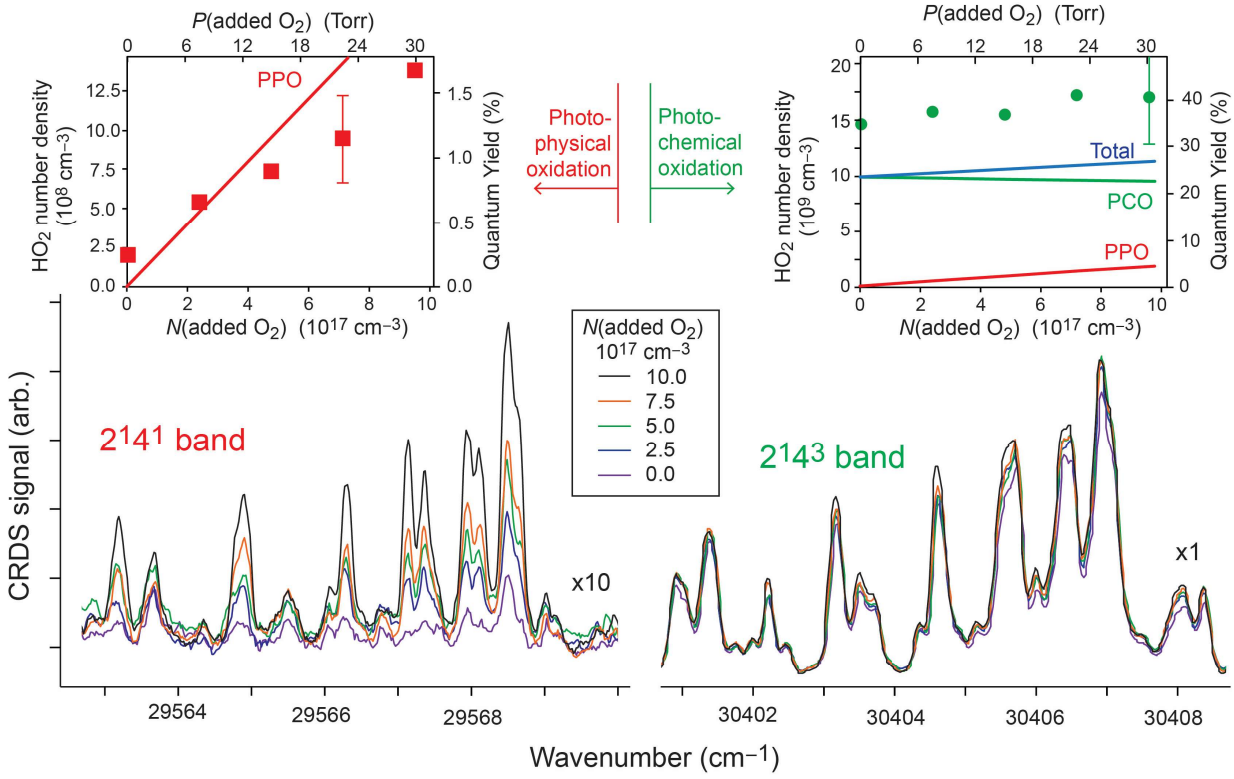

Fig. 3. The pressure dependence of HO_2 formation. Main figure: action spectra of HCHO via the $2^1 4^1$ and $2^1 4^3$ levels as a function of added O_2 at 50 Torr total pressure (balance He). Insets: HO_2 number density and relative quantum yields as a function of O_2 pressure for each level. Points: Experimental with example error bar attached to only one point. Lines: ME Model.

of magnitude larger than the radical density, all reaction conditions are pseudo first-order and any H and HCO radicals formed from R1 should quantitatively form HO_2 via R3 and R4, that is, via

the conventional PCO mechanism. The slight increase in HO_2 as *P*(added O_2) is increased may be due to the presence of the PPO channel (R5) and/or reduced diffusion of H-atoms and HO_2 to the reactor walls and this is tested below.

End-product analysis using FTIR spectroscopy: Figure 4 shows FTIR product spectra, following 5 min irradiation of 1.0 Torr neat HCHO at 338.39 nm ($2^1 4^1$, below the photochemical threshold for radical formation), as well as diluted in 160 Torr N_2, 160 Torr O_2 and 760 Torr synthetic air (79% N_2, 21% O_2). The parent HCHO spectrum has been subtracted, revealing only features of photolysis products. The asterisks show where a residual, sharp HCOH Q-branch feature has been manually removed. The saturation of this Q-branch at low pressure causes a small non-linear pressure dependence and so is difficult to completely subtract. Similar spectra following excitation to the HCHO 4^1 (352.48 nm) and $2^1 4^3$ (329.06 nm) levels in synthetic air are shown in Fig. S1. The FTIR spectra for neat HCHO photolysis, and in the presence of N_2, show only CO, which is formed via R2 (the H_2 co-product does not absorb IR light). The FTIR product spectra taken in the presence of O_2 show an additional product: formic acid, HCOOH. The presence of HCOOH can be explained via the known reaction scheme (*26*, *32*, *33*):

$$HO_2 + HCHO \overset{M}{\rightleftharpoons} HOCH_2O_2 \rightarrow\rightarrow HCOOH \qquad \text{(R6)}$$

where M is a buffer gas, and HO_2 has been assumed, previously, to have formed via PCO. The double arrow indicates that a sequence of elementary reactions leading to HCOOH, and these are expanded in supplementary information (Fig. S2). The observation of HCOOH as an end-product, following excitation to the HCHO $2^1 4^1$ and 4^1 levels in 760 Torr synthetic air (Figs 4 and S1, respectively), confirms production of HO_2, at pressures relevant in the troposphere, at excitation energies below the HCHO radical threshold.

Discussion

Our experimental results present a convincing case that low energy photo-excitation of HCHO allows it to react with O_2. The CRDS experiments demonstrate HO_2 is formed at energies up to 24 kJ mol^{-1} below the radical threshold. The FTIR experiments at 1 Bar pressure of air show formation of HCOOH below the radical threshold, consistent with reaction between HO_2 and the

parent HCHO. The linear dependence of HO_2 with O_2 concentration seen in the CRDS experiments implies a bimolecular reaction between photo-excited HCHO and O_2.

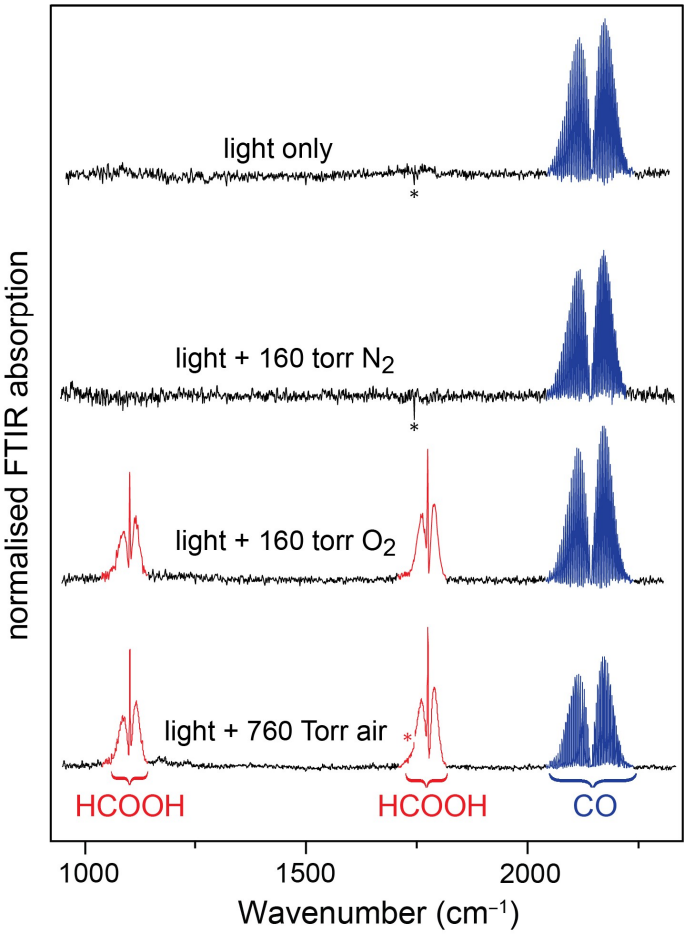

Fig. 4: FTIR spectra of reaction end products following excitation of 1 Torr HCHO to the $2^1 4^1$ level in different buffer gases as indicated. Spectra are on the same scale but displaced vertically for presentation. HCOOH is only formed in the presence of O_2. The asterisks show where a sharp residual HCHO Q-branch feature remains even after subtraction of parent spectrum.

The PPO mechanism: Three HCHO electronic states could be involved in reaction with O_2: *i)* the initially prepared S_1 state, *ii)* the T_1 state, formed after intersystem crossing (ISC), or *iii)* highly vibrationally excited states of S_0, formed following internal conversion (IC) from S_1.

Reaction with HCHO (T_1) is highly unlikely. HCHO is a small molecule in radiationless transition theory (*34*) – the density of states in its triplet manifold is very sparse at our experimental energies. Consequently, the ISC rate is strongly dependent on the initially excited HCHO rotation-vibration level. For the levels we consider, this manifests in highly variable fluorescence lifetimes, which vary by more than two orders of magnitude (*35*), and markedly different reaction dynamics, varying between T_1- and S_0-dominated reaction (*9*, *36*). The HO_2 action spectrum in Fig. 2, however, shows an intensity pattern that is fit well for each vibrational level, at the level of individual rotational states, by a single simulated absorption spectrum. This implies a uniform (constant) relationship between the HCHO levels excited and the production of HO_2, allowing us to discount HCHO (T_1) as the reactive species. This conclusion is consistent with previous investigations of the photophysics of HCHO at these energies (*37*).

Reaction of O_2 with HCHO (S_1) correlates with HCO in the electronically excited $\tilde{A}(^2A')$ state. Although the HCO($\tilde{A}$) + HO_2 products are energetically accessible, the $\tilde{A}$ state of HCO is linear and this nuclear rearrangement will result in a significant energy barrier. We observe HO_2 and HCOOH following excitation of the lowest accessible HCHO (S_1) state, 4^1, with $\nu_4' = 124.5$ cm^{-1} (*30*). In addition, the PPO QY (see below) is the same, within error, for the $2^1 4^1$ and 4^1 states, even though the 4^1 state is ~1200 cm^{-1} lower in energy. This suggests a critical energy for PPO that is far below the 4^1 state, rather than one with a significant barrier. Although we cannot definitively rule it out, HCHO (S_1) reaction is unlikely because the reaction barrier is expected to be significantly higher than the available energy of the colliding molecules.

The remaining possibility is that reaction occurs between highly vibrationally excited, S_0 HCHO (HCHO‡) and O_2:

$$\mathrm{HCHO} + h\nu \rightarrow \mathrm{HCHO}\ (S_1) \xrightarrow{\mathrm{IC}} \mathrm{HCHO}^‡\ (S_0) \xrightarrow{O_2} \mathrm{HO_2} + \mathrm{HCO} \qquad \text{(PPO)}$$

HCHO‡ has extremely high, non-thermal, vibrational energy arising from absorption of a photon but all other degrees of freedom, including the HCHO and O_2 translational and rotational energy, are thermalised at ~300 K.

Theoretical validation of the PPO mechanism: There has been one previous theoretical study of R5 (*38*), which indicates a zero-point corrected barrier between 152 and 155 kJ/mol and a dipole-bound complex in the exit channel. We have re-examined the energetics of R5 using electronic structure theory. Details and discussion of these calculations are provided as supplementary

information. The lowest energy saddle point for R5 corresponds to an anti-periplanar orientation of the O_2 with respect to the C=O bond in HCHO. The threshold energy is sensitive to the level of electronic structure theory used and we calculate a range of 151.0 – 175.4 kJ mol^{-1}, with a recommended zero-point corrected value of 161.4 kJ mol^{-1}, both of which are shown in Fig. 1. At many levels of theory, the R5 saddle point is submerged, consistent with barrierless reverse reaction (*39*, *40*).

The 'late' saddle point for R5 and the small energy difference between optimised anti-periplanar and syn-periplanar saddle points (Tables S2 and S3) suggest the potential energy surface in the vicinity of the saddle point is relatively flat with respect to O_2 in- and out-of-plane rotation, that is, O_2 can react with HCHO at almost any angle. Combined with our recommended threshold energy and the reaction enthalpy (*6*), this suggests PPO is energetically feasible and likely very efficient. Indeed R5 has been found to be efficient in shock tube experiments (*39-43*), although here all degrees of freedom, including relative translation and rotation, are in thermal equilibrium at elevated temperature.

PPO quantum yields: We determine ϕ_{PPO} in CRDS experiments by internal calibration. Above the R1 threshold, photo-excitation results in two HO_2 radicals, via R3 and R4 with known QY, ϕ_1 = 0.40 ± 0.06 at λ = 329 – 331 nm. The radical QY is reported to be pressure-independent (*24, 25*). We do observe a weak pressure dependence for this channel, however the variation is within the uncertainty of the literature measurements and we use ϕ_1 = 0.40 ± 0.06 as our internal calibration. The PPO reaction also produces two HO_2 radicals, via R5 and R4. We calculate ϕ_{PPO} from the ratio of the observed HO_2 number density following excitation of the lower energy levels, compared to the 2^14^3 level. The HCHO absorption cross-section for each transition is known and corrected for, which then yields the wavelength-dependent QY, ϕ_{PPO}. At 30 Torr added O_2, we determine ϕ_{PPO} = 0.017 ± 0.005 at 338 nm (2^14^1), 0.025 ± 0.010 at 343 nm (4^3) and 0.014 ± 0.007 at 352 nm (4^1), where the uncertainty arises from the combined uncertainty of the fit to literature absorption spectra and the uncertainty in the literature QY of the 2^14^3 level. Details of these calculations are provided as SM.

Extraction of the PPO QY in FTIR experiments is challenging because the experiments measure the HCOOH end-product, whereas, as shown Fig. S2, HO_2 production following PCO and PPO is catalytic. Therefore measured HCOOH QYs do not reflect the primary QY for PCO or PPO.

Master Equation modelling of HO_2 formation

A Master Equation (ME) model was developed, as described in SI, to simulate the CRDS experiments. The model includes IC of HCHO from S_1 to S_0 and collisional energy transfer within the S_0 and S_1 electronic states. The T_1 state was not included. As discussed above, there is no evidence of the involvement of T_1 and, further, IC is known to be the dominant non-radiative relaxation mechanism in HCHO (*37*). Reactions R1, R2 and R5 were used to calculate QYs for H + HCO, H_2 + CO and HCO + HO_2.

The IC rate coefficients were determined from the experimentally observed non-radiative lifetimes of the distinct HCHO S_1 states (*37*). Microcanonical molecular channel rate coefficients for R2 were taken as the $J = 10$ rate coefficients, as calculated by Troe (*11*). These rate coefficients include anharmonic corrections and parabolic tunnelling, with a $J = 0$ barrier height of 342.6 kJ mol^{-1} (*11, 44*). As described in SI, Troe's expression for the R1 radical channel QY (*11*) was refit to the available experimental data and used to obtain a microcanonical rate coefficient for R1.

Two methods were used to model the PPO rate coefficient – a bottom-up approach calculating k_{PPO} from first principles, and a top-down empirical approach fitting k_{PPO} to the experimental data using an assumed functional form. The bottom-up approach used the semi-microcanonical method of Maranzana *et al* (*45*). Here the internal energy distribution of the HCHO is microcanonical, corresponding to the laser excitation wavelength, and all other degrees of freedom are treated thermally. The empirical top-down method assumes k_{PPO} will be exponential with energy in the energy range considered with the intercept and exponent varied to minimise the least squares difference to experimental data obtained below the radical threshold.

The four different microcanonical rate coefficients considered are plotted as a function of internal (photolysis) energy in Fig. 5A.

Pressure-dependent reactant and product populations were modelled using a one-dimensional ME simulation in energy, as implemented in the Multiwell program package (*46-48*). A simple exponential energy transfer model was employed (*11*) together with Lennard-Jones collision frequencies for N_2 and O_2 at 300 K. The average downward collisional energy transfer is taken to be $\langle \Delta E_{down} \rangle = 250$ cm^{-1} for collisions of S_0 HCHO with N_2 and O_2 and $\langle \Delta E_{down} \rangle = 25$ cm^{-1} for collisions of S_1 HCHO with N_2 and O_2, reflecting the sparse density of states in S_1. The ME simulations were run with 150,000 stochastic trials for 1.0 μs, that is, for less than the duration

between laser pulses, with the final populations of each species being stable. More details of the ME modelling are provided as SI.

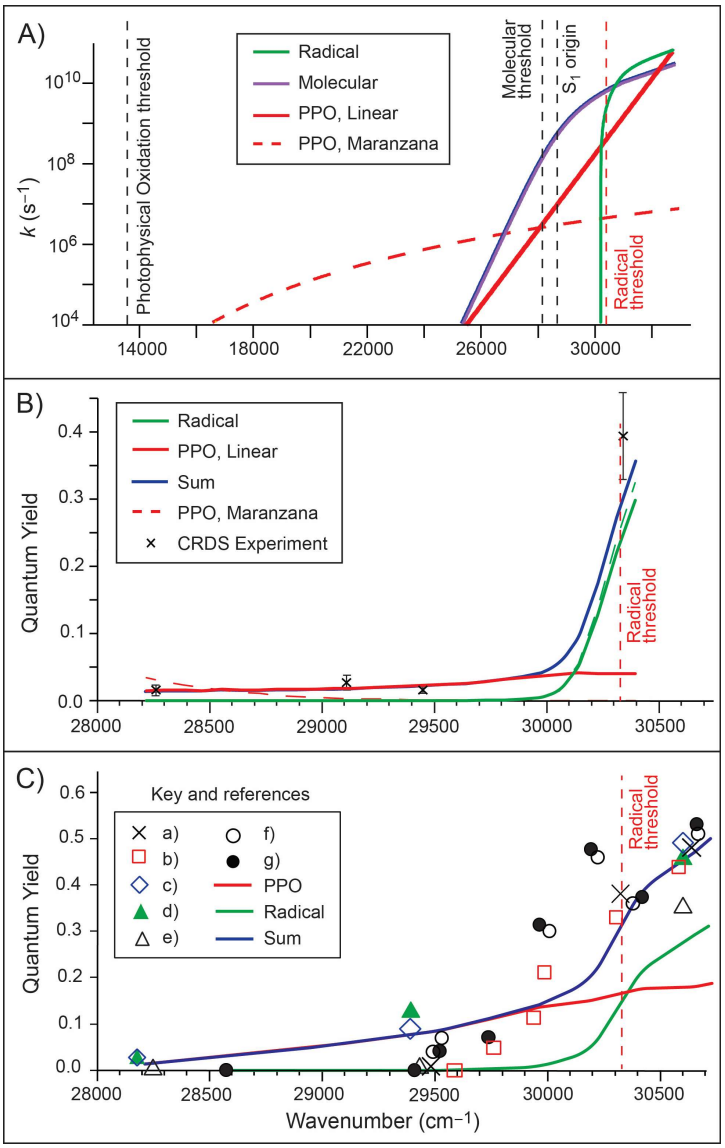

Fig. 5: Energy dependence of rate coefficients and quantum yields. A) First order, microscopic rate coefficients used in Master Equation calculations. The PPO rate coefficient is pseudo first order for 30 Torr O_2. B) Quantum yields for various processes in CRDS experiments at 30 Torr added O_2. C) Quantum yields at atmospheric pressure. a) Ref 18; b) Ref 19; c) Ref 20; d) Ref 21; e) Ref 22; f) Ref 23; g) Ref 24

Figure 5B shows ME results for the CRDS conditions at 30 Torr O_2, 20 Torr He. The Maranzana form (*45*) of the PPO rate coefficient yields ϕ_{PPO} that is close to experiment at the lowest 4^1 level. However ϕ_{PPO} drops with increasing energy and is essentially zero for the other two experimental energies. At higher energies, as seen in Fig. 5A, the R2 molecular channel rate coefficient rises

more steeply with energy in this region and out-competes the Maranzana k_{PPO}. This is not in accord with the experimental findings.

The energy-dependent HO_2 QYs obtained with k_{PPO} fit to the experimental data, solid red line in Fig. 5B, are within error of the CRDS experimental data below the radical threshold. When PPO is added to the radical channel QY, the overall radical yield is also in acceptable agreement with experiment at the $2^1 4^3$ energy.

The ME simulations have also been used to predict the O_2 pressure dependence of the HO_2 QY (Fig. 3 and Table S8). The observed CRDS pressure dependence is modelled well, using the fitted k_{PPO}, with the strong linear increase in HO_2 QY with pressure reproduced for states below the radical threshold. The ME simulations also predict a much weaker linear increase in HO_2 QY with pressure for the $2^1 4^3$ state, where PCO via the radical channel products dominates HO_2 production. Indeed the ME simulations predict, with increasing pressure, a slight quenching of the PCO QY and an enhancement of PPO.

Energy dependent QYs from ME simulations at 1 Bar pressure, using the fitted k_{PPO}, are shown in Fig. 5C. These compare well to experimental radical channel QYs, for energies near to and below the radical channel threshold.

Although the exponential form of k_{PPO} fits the CRDS and 1 Bar pressure experimental QY data well, caution should be exercised. Extrapolating to higher energies, the empirical exponential form causes PPO to dominate, exceeding even the unimolecular radical rate, which is unreasonable. Further, $k_{PPO}(E)$ must be bounded by the collision encounter rate. At lower energies the empirical form of k_{PPO} drops too quickly. The PPO energy threshold is ~13,500 cm^{-1} (Fig. 5A), with an entrance channel that is very flat. This suggests, as found in shock tube experiments (*39*,*43*), PPO is likely to be efficient, even near threshold. The form of the Maranzana $k_{PPO}(E)$ is therefore more reasonable at lower energies. These observations indicate that the energy dependence of k_{PPO} is more complex than a single exponential function.

Formaldehyde has two well-known complexities in its dynamics, occurring just below the energy of the radical channel. Firstly, the barrier to isomerisation to hydroxymethylene (CHOH) lies near 30,000 cm^{-1} (*49*,*50*) with tunnelling reducing the effective barrier. Secondly, the roaming dynamical pathway links the radical and molecular channels, with a threshold about 60 cm^{-1} below the radical threshold (*51*). The roaming mechanism involves a loosely bound H-atom on a flat region of the potential energy surface. Both of these mechanisms provide reasonable

explanations for an increase in $k_{PPO}(E)$ over the Maranzana single well calculation, in particular increasing k_{PPO} as the radical threshold is approached. A loosely bound H atom can be easily abstracted by O_2 and CHOH can also undergo PPO. Calculation of these additional microcanonical rate coefficients is beyond the scope of the present study.

.

Comparison with previous HCHO measurements and atmospheric implications: The previously reported radical quantum yields for excitation of HCHO at $\lambda > 330$ nm are highly varied and dependent on conditions, as described in SI. Early experiments showed considerable radical yield at long wavelengths, which was then attributed to a lower R1 threshold energy than is now accepted (*52-55*). In the late 1970s and 80s, when the radical threshold was established close to where it is today (*8*), the groups of Calvert (*18*) and Moortgat/Warneck (*21, 22)* used measurements of CO and H_2 yields (R2) to infer ϕ_1 by difference. Two studies (*18, 21*) found ϕ_1 = 0.03 to 0.05 near 336 nm, reducing to near zero at 340 nm, while the third (*22*) argued for no radical quantum yield below the R1 threshold. Later, Smith, *et al*. measured the HCO radicals directly, and reported $\phi_1 = 0.07$ at 336 nm and 0.04 at 339 nm (*23*). These results are shown in Fig. 5C. In addition, the production of HCOOH following photolysis of HCHO has also been reported previously for $\lambda > 330$ nm (*21,26*). No interpretation has been offered for the presence of radicals, nor HCOOH, at photolysis energies below the radical threshold. We propose HCOOH is formed from HO_2 arising from PPO. Given our observation of the sensitivity of PPO to trace amounts of O_2 (Fig. 3), the observed quantum yields and observation of HCOOH over many years are broadly consistent with our reported ϕ_{PPO}.

This work proposes that the radical quantum yields currently used in atmospheric modelling (*24*) invoke the wrong mechanism for $\lambda > 330$ nm. However, because the PPO of HCHO produces the same radical species as direct PCO, the implications for tropospheric chemistry will be subtle. The only consequence will be the different pressure dependences of the R1 and R5 pathways; the R1 QY decreases with pressure whereas the R5 QY increases with pressure. For more complex molecules, however, the PCO and PPO mechanisms will produce different radicals, with different consequences.

The photochemical properties of HCHO are not unique nor special other than the simplicity imbued by a small number of atoms. We predict other molecules will have competitive PPO pathways. For example, there is unrecognised evidence of PPO in the photochemistry of acetaldehyde, CH_3CHO. Morajkar *et al.* used CRDS to investigate HO_2 production following photolysis of CH_3CHO at 248 nm (*56*). They identified HO_2 arising via PCO *via* the HCO + CH_3 and CH_3 + CO + H dissociation channels. They also identified a third "rapid HO_2" pathway with no known mechanism, speculating HO_2 was formed from reaction of O_2 with photo-excited CH_3CHO. This is a description of the PPO reaction and we propose Morajkar *et al.* measured PPO in CH_3CHO and that the "energetic CH_3CHO" speculated in that paper is a highly vibrationally excited S_0 molecule, arising via non-radiative relaxation from the initially exited S_1 CH_3CHO. Their reported quantum yield of 0.07 is consistent with the ϕ_{PPO} we have determined for HCHO.

In CH_3CHO, the dominant PCO pathway is *via* CH_3 + HCO radical channel. PPO would instead lead to CH_3CO + HO_2 where the acetyl radicals can subsequently form peroxyacetylnitrate (PAN), especially in urban areas (*1,2*). As such, the PPO route is more similar to the reaction of CH_3CHO with OH radicals where the aldehydic H-atom is abstracted to form H_2O + CH_3CO. The difference in these mechanisms is that OH reaction results in a nett loss of HO_x radicals (HO_x = OH + HO_2) from the atmosphere. Conversely, PPO results in a nett gain in HO_x radicals via direct formation of HO_2.

We also suggest PPO may be important in carbonyls more generally, and particularly in carbonyls with low photolysis QYs. Such atmospherically important carbonyls include acetone, the highest mostly highly emitted industrial ketone with 44 Tg/yr emitted to the atmosphere (*57*), and methylvinylketone and methacrolein, which are major oxidation products of isoprene, the largest emitted biogenic compound in the troposphere (*58*). Many other molecules also satisfy the conditions for PPO, including alkyl- and aryl-nitrates, NO_2 itself, and alkylperoxides. If PPO is occurring in these and other molecules, the implications for tropospheric chemistry include:

i) Formation of different radicals than previously considered, which may have different subsequent fates and impact. Generally, PPO will produce larger radicals *via* H-abstraction compared to photolysis, which frequently breaks a C-C bond The larger carbon-centred radicals formed by PPO will react with atmospheric O_2 to form less volatile oxygenated species that are implicated in aerosol formation (***Erreur ! Signet non défini.***).

ii) Radical formation at lower photon energies, below radical dissociation thresholds. Radicals formed via PPO will affect the modelled mixing ratio of radical chain carriers, for example OH and HO_2.

iii) Changes to the vertical profile for radical formation. Photolysis quantum yields quench with increasing pressure, as collisional relaxation competes with unimolecular reaction; ϕ_{ph} are highest at low pressure. However, as a bimolecular reaction, PPO quantum yields will increase with increasing O_2 partial pressure (Fig. 3 and Table S8).

We propose PPO will be a general reaction in atmospheric chemistry. Any molecule that absorbs absorb near-UV light, has small fluorescence and photolysis QYs and has a low energy abstraction pathway for reaction with O_2 is likely to undergo PPO. Many atmospherically prevalent molecules satisfy these criteria including carbonyls, alkyl- and aryl-nitrates, NO_2 itself, and alkylperoxides.

Conclusions

We have identified photophysical oxidation (PPO) in the photochemistry of HCHO in the presence of O_2. The PPO reaction involves photo-excitation of the parent molecule, its non-radiative transfer to the electronic ground state and subsequent fast reaction with O_2, before the molecule has a chance to thermalise. PPO is a single elementary reaction and can occur at photon energies below radical dissociation thresholds, whereas conventional photochemical oxidation requires an initial radical photolysis, so can only occur at photon energies above the radical threshold, and refers to multiple elementary reactions. As a bimolecular reaction, the PPO reaction rate increases with O_2 pressure, which is the reverse to normal photolysis, where increased pressure generally quenches the reaction. In the atmosphere, PPO is therefore more important at higher pressures, that is, at lower altitudes, relative to other photochemical processes.

Photophysical oxidation is likely to be a general reaction in tropospheric chemistry and its implications are yet to be explored.

Acknowledgements:

The authors thank C. Hecquet and C. Schoemaecker for assistance with the Lille photolysis laser. BW and MC acknowledge Australian government Research Training Scheme scholarships.

Funding:

Australian Research Council grant DP190102013. (BW, MC, PS, KN, MJTJ, SHK)

French ANR agency under contract No. ANR-11-Labx-0005-01 CaPPA (Chemical and Physical Properties of the Atmosphere) (EA, CF)

The Région Hauts-de-France, the Ministère de l'Enseignement Supérieur et de la Recherche (CPER Climibio) (EA, CF)

European Fund for Regional Economic Development. (EA, CF)

Computation was supported with the assistance of resources from the National Computational Infrastructure (NCI Australia), an NCRIS enabled capability supported by the Australian Government. (MC, MJTJ)

Author contributions:

Conceptualization: MJTJ, SHK

Methodology and investigation: BW, MC, EA, KN, PS, MJTJ, CF, SHK

Funding acquisition, project administration: MJTJ, CF, SHK

Supervision: KN, MJTJ, CF, SHK

Writing – original draft: MJTJ, SHK

Writing – review & editing: BW, MC, EA, KN, PS, MJTJ, CF, SHK

Competing interests: The authors declare that they have no competing interests.

Data and materials availability: All data are available in the manuscript or the supplementary materials.

Supplementary Materials

Materials and Methods

Supplementary Text

Tables S1 – S8

Figs S1 – S12

Additional References (*59-87*)

References

1. for example, B. J. Finlayson-Pitts, J. N. Pitts, Jr. *Chemistry of the Upper and Lower Atmosphere – Theory, Experiments, and Applications*, (Academic Press, San Diego, CA, 2000).

2. R. Atkinson, J. Arey, Atmospheric Degradation of Volatile Organic Compounds. *Chem. Rev.* **103**, 4605−4638 (2003). doi.org/10.1021/cr0206420

3 D. R. Glowacki, J. Lockhart, M. A. Blitz, S. J. Klippenstein, M. J. Pilling, S. H. Robertson, P. W. Seakins, Interception of excited vibrational quantum states by O_2 in atmospheric association reactions, *Science*, **337**, 1066 (2012)

4 V. Vaida, D. J. Donaldson, Red-light initiated atmospheric reactions of vibrationally excited molecules, *Phys. Chem. Chem. Phys.* **16**, 827–836 (2014)

5. e.g. J. C. Tully, Reactions of O(^1D) with atmospheric molecules. *J. Chem. Phys*. **62**, 1893–1898 (1975); doi.org/10.1063/1.430675

6. B. Ruscic and D. H. Bross, Active Thermochemical Tables (ATcT) values based on ver. 1.124 of the Thermochemical Network (2022); available at ATcT.anl.gov; accessed 20 December 2022.

7. P. L. Houston, C. B. Moore, Formaldehyde photochemistry: Appearance rate, vibrational relaxation, and energy distribution of the CO product. *J. Chem. Phys.* **65**, 757–770 (1976). doi.org/10.1063/1.433092

8. M.-C. Chuang, M. F. Foltz, C. B. Moore, T_1 barrier height, S_1–T_1 intersystem crossing rate, and S_0 radical dissociation threshold for HCHO, D_2CO, and HDCO. *J. Chem. Phys.* **87**, 3855–3864 (1987). doi.org/10.1063/1.452940

9. L. R. Valachovic, M. F. Tuchler, M. Dulligan, Th. Droz-Georget, M. Zyrianov, A. Kolessov, H. Reisler, C. Wittig, Photoinitiated HCHO unimolecular decomposition: Accessing H+HCO products via S_0 and T_1 pathways. *J. Chem. Phys.* **112**, 2752–2761 (2000). doi.org/10.1063/1.480849

10. D. Townsend, S. A. Lahankar, S. K. Lee, S. D. Chambreau, A. G. Suits, X. Zhang, J. Rheinecker, L. B. Harding, J. M. Bowman, The roaming atom: Straying from the reaction path in formaldehyde decomposition. *Science* **306**, 1158–1161 (2004). doi.org/10.1126/science.1104386

11. J. Troe, Analysis of Quantum Yields for the Photolysis of Formaldehyde at $\lambda > 310$ nm. *J. Phys. Chem. A* **111**, 3868–3874 (2007). doi.org/10.1021/jp066886w

12. M. S. Quinn, K. Nauta, M. J. T. Jordan, J. M. Bowman, P. L. Houston, S. H. Kable, Rotational resonances in the HCHO roaming reaction are revealed by detailed correlations, *Science*, **369**, 1592–1596 (2020). doi.org/10.1126/science.abc4088

13. M. S . Quinn, D. U. Andrews, K. Nauta, M. J. T. Jordan, S. H. Kable, The energy dependence of CO(v, J) produced from via the transition state, roaming, and triple fragmentation channels. *J. Chem. Phys.* **147**, 013935 (2017). doi.org/10.1063/1.4983138

14. D. Feller, M. Dupuis, B. C. Garrett, Barrier for the HCHO → H_2 + CO reaction: A discrepancy between high-level electronic structure calculations and experiment. *J. Chem. Phys.* **113**, 218–226, (2000). doi.org/10.1063/1.481788

15. G. F. Bauerfeldt, L. M.M. de Albuquerque, G. Arbilla, E. C. da Silva, Unimolecular reactions on formaldehyde S_0 PES. *J. Molec. Struct. (Theochem)* **580**, 147–160 (2002). doi.org/10.1016/S0166-1280(01)00609-1

16. X. Zhang, J. L. Rheinecker, and J. M. Bowman, Quasiclassical trajectory study of formaldehyde unimolecular dissociation: HCHO → H_2 + CO, H + HCO. *J. Chem. Phys.* **122**, 114313 (2005). doi.org/10.1063/1.1872838

17. L. B. Harding, S. J. Klippenstein, A. W. Jasper, Ab initio methods for reactive potential surfaces. *Phys. Chem. Chem. Phys*. **9**, 4055–4070 (2007). doi.org/10.1039/B705390H

18. J. H. Clark. C. B. Moore, N. S. Nogar, *J. Chem. Phys.* **68**, 1264–1271 (1978). doi.org/10.1063/1.435848

19. A. Horowitz, J. G. Calvert, Wavelength dependence of the quantum efficiencies of the primary processes in formaldehyde photolysis at 25°C. *Int. J. Chem. Kin*. **10**, 805–819 (1978). doi.org/10.1002/kin.550100803

20. G. K. Moortgat, F. Slemr, W. Seiler, P. Warneck, Relative quantum yields of H_2 and CO in the wavelength range 70-360 nm. *Chem. Phys*. *Lett.* **54**, 444–447 (1978). doi.org/10.1016/0009-2614(78)85257-9

21. G. K. Moortgat, P. Warneck, CO and H_2 quantum yields in the photodecomposition of formaldehyde in air. *J. Chem. Phys.* **70**, 3639–3651 (1979). doi.org/10.1063/1.437956

22. G. K. Moortgat, W. Seiler, P. Warneck, Photodissociation of HCHO in air: CO and H_2 quantum yields at 220 and 300 K. *J. Chem. Phys.* **78**, 1185–1190 (1983). doi.org/10.1063/1.444911

23. G. D. Smith, L. T. Molina, M. J. Molina, Measurement of radical quantum yields from formaldehyde photolysis between 269 and 339 nm. *J. Phys. Chem. A.* **106**, 1233–1240 (2002). doi.org/10.1021/jp-13180n

24. R. Atkinson, D. L. Baulch, R. A. Cox, J. N. Crowley, R. F. Hampson, R. G. Hynes, M. E. Jenkin, M. J. Rossi, J. Troe, Evaluated kinetic and photochemical data for atmospheric chemistry: Volume II gas phase reactions of organic species. *Atmos. Chem. Phys*. **6**, 3625–4055 (2006). doi.org/10.5194/acp-6-3625-2006; IUPAC Subcommittee for Gas Kinetic Data Evaluation, (http://iupac.pole-ether.fr). Datasheet updated: 16th April 2013; last change in preferred values: 16th April 2013

25. J. S. Campbell, K. Nauta, C. S. Hansen, S. H. Kable, POPTARTS: A New Method to Determine Quantum Yields in a Molecular Beam, *J. Phys. Chem. A,* **XX**, XXXX (2022) (published on-line 30-Nov-2022). doi.org/10.1021/acs.jpca.2c06289

26. F. Su, J. G. Calvert, J. H. Shaw, Mechanism of the photooxidation of gaseous formaldehyde. *J. Phys. Chem*. **83**, 3185–3191 (1979). doi.org/10.1021/j100488a001

27. A. C. Terentis, S. E. Waugh, G. F. Metha, S. H. Kable, HCO (N, K_a, K_c, J) distributions from near-threshold photolysis of HCHO (J, K_a, K_c). *J. Chem. Phys*. **108**, 3187–3198 (1998). doi.org/10.1063/1.475736

28. E. Assaf, L. Liu, C. Schoemaecker, C. Fittschen, Absorption Spectrum and Absorption Cross Sections of the $2\nu_1$ band of HO_2 between 20 and 760 Torr Air in the Range 6636 and 6639 cm^{-1}. *J. Quant. Spectrosc. & Rad. Transfer* **211**, 107–114 (2018). doi.org/10.1016/j.jqsrt.2018.02.035

29. M. F. Shaw, B. Sztáray, L. K. Whalley, D. E. Heard, D. B. Millet, M. J. T. Jordan, David L. Osborn, S. H. Kable, Photo-tautomerization of acetaldehyde as a photochemical source of formic acid in the troposphere. *Nat. Commun.,* **9**, 2584 (2018). doi.org/10.1038/s41467-018-04824-2

30. D. J. Clouthier, D. A. Ramsay, The spectroscopy of formaldehyde and thioformaldehyde. *Ann. Rev. Phys. Chem*. **34**, 31–58 (1983). doi.org/10.1146/annurev.pc.34.100183.000335

31. M. Motsch, M. Schenk, M. Zeppenfeld, M. Schmitt, W. L. Meerts, P. W. H. Pinkse, G. Rempe, Spectroscopy of the A^1A_2 - X^1A_1 transition of formaldehyde in the 30140 – 30790 cm^{-1} range: The $2^1_0 4^3_0$ and $2^2_0 4^1_0$ rovibrational bands. *J. Molec. Spectrosc*. **252,** 25–30 (2008). doi.org/10.1016/j.jms.2008.06.002

32. M. E. Jenkin, M. D. Hurley, T. J. Wallington, Investigation of the radical product channel of the $CH_3C(O)O_2 + HO_2$ reaction in the gas phase. *Phys. Chem. Chem. Phys*. **9**, 3149–3162 (2007). doi.org/10.1039/B702757E

33. P. Morajkar, C. Schoemaecker, M. Okumura, C. Fittschen, Direct measurement of the equilibrium constants of the reaction of formaldehyde and acetaldehyde with HO_2 radicals. *Int. J. Chem. Kin.* **46**, 245–259 (2014). doi.org/10.1002/kin.20817

34. M. Bixon, J. Jortner, Intramolecular radiationless transitions. *J. Chem. Phys.* **48**, 715–726 (1968). doi.org/10.1063/1.1668703

35. J. C. Weisshaar, C. B. Moore, Isotope, electric field, and vibrational state dependence of single rotational level lifetimes of S_1 formaldehyde. *J. Chem. Phys*. **72**, 5415–5425 (1980). doi.org/10.1063/1.439036

36. H. M. Yin, S. H. Kable, X. Zhang, J. M. Bowman, Signatures of HCHO photodissociation from two electronic states. *Science* **311**, 1443–1446 (2006). doi.org/10.1126/science.1123397

37. R. G. Miller, E. K. C. Lee, Single vibronic level photochemistry of formaldehydes in the $\tilde{A}\ ^1A_2$ state: Radiative and nonradiative processes in HCHO, HDCO, and D_2CO. *J. Chem. Phys.* **68**, 4448–4464 (1978). doi.org/ 10.1063/1.435527

38. L. K. Huynh, M. Tirtowidjojo, T, N. Truong, Theoretical study on kinetics of the $HCHO + O_2 \rightarrow HCO + HO_2$ reaction. *Chem. Phys. Lett.* **469**, 81–84 (2009). doi.org/10.1016/j.cplett.2008.12.050

39. J. V. Michael, S. S. Kumaran, M.-C. Su, Rate constants for $CH_3 + O_2 \rightarrow CH_3O + O$ at high temperature and evidence for $HCHO + O_2 \rightarrow HCO + HO_2$. *J. Phys. Chem. A* **103**, 5942–5948 (1999). doi.org/10.1021/jp9909457

40. V. Vasudevan, D. F. Davidson, R. K. Hanson, C. T. Bowman, D. M. Golden, High-temperature measurements of the rates of the reactions $CH_2O + Ar \rightarrow$ products and $CH_2O + O_2 \rightarrow$ products. *Proc. Comb. Inst*. **31***,* 175–183 (2007)*.* doi.org/10.1016/j.proci.2006.07.017

41. Y. Hidaka, T. Taniguchi, H. Tanaka, T. Kamesawa, K. Inami, H. Kawano, Shock-tube study of CH_2O pyrolysis and oxidation. *Combut. Flame* **92**, 365–376 (1993). doi.org/10.1016/0010-2180(93)90149-W

42. B. Eiteneer, C.-L. Yu, M. Goldenberg, M. Frenklach, Determination of rate coefficients for reactions of formaldehyde pyrolysis and oxidation in the gas phase. *J. Phys. Chem. A* **102**, 5196-5205 (1998). doi.org/10.1021/jp981184v

43. N. K. Srinivasan, M.-C. Su, J. W. Sutherland, J. V. Michael, Reflected shock tube studies of high-temperature rate constants for $CH_3 + O_2$, $HCHO + O_2$, and $OH + O_2$. *J. Phys. Chem. A*, **109**, 7902–7914 (2005). doi.org/10.1021/jp0581330

44. D. Feller, M. Dupuis B. C. Garrett, Barrier for the reaction: A discrepancy between high-level electronic structure calculations and experiment *J. Chem. Phys*. **113**, 218–226 (2000); doi.org/10.1063/1.481788

45. A. Maranzana, J. R. Barker, G. Tonachini, Master equation simulations of competing unimolecular and bimolecular reactions: application to OH production in the reaction of acetyl radical with O_2. *Phys. Chem. Chem. Phys.* **9**, 4129–4141 (2007). doi.org/10.1039/b705116f

46. J. R. Barker, T. L. Nguyen, J. F. Stanton, C. Aieta, M. Ceotto, F. Gabas, T. J. D. Kumar, C. G. L. Li, L. L. Lohr, A. Maranzana, N. F. Ortiz, J. M. Preses, J. M. Simmie, J. A. Sonk, and P. J. Stimac; MultiWell-2022 Software Suite; J. R. Barker, University of Michigan, Ann Arbor, Michigan, USA, 2022; http://clasp-research.engin.umich.edu/multiwell/.

47. J. R. Barker*,* Multiple-Well, multiple-path unimolecular reaction systems. I. MultiWell computer program suite. *Int. J. Chem. Kinetics,* **33***,* 232–245 (2001). doi.org/ 10.1002/kin.1017

48. J. R. Barker*,* Energy transfer in master equation simulations: A new approach. *Int. J. Chem. Kinetics,* **41**, 748–763 (2009)*.* doi.org/ 10.1002/kin.20447

49. X. Zhang, S. Zou, L. B. Harding, J. M. Bowman, A Global *ab Initio* Potential Energy Surface for Formaldehyde, *J. Phys. Chem. A.* **108**, 8980–8986 (2004).

50. S. Maeda, K. Ohno, K. Morokuma, Automated global mapping of minimal energy points on seams of crossing by the anharmonic downward distortion following method: A case study of H_2CO, *J. Phys. Chem. A*, **113**, 1704–1710 (2009). doi.org/10.1021/jp810898u

51. S. A. Lahankar, S. D. Chambreau, X. Zhang, J. M. Bowman, A. G. Suits, Energy dependence of the roaming atom pathway in formaldehyde decomposition, *J. Chem. Phys.* **126**, 044314 (2007). doi.org/10.1063/1.2429660

52. R. Klein, L. J. Schoen, Photodecomposition of formaldehyde; stability of the HCO radical. *J. Chem. Phys.* **24**, 1094-1096 (1956). doi.org/10.1063/1.1742685

53. M. Venugopalan, K. O. Kutschke, The photolysis of formaldehyde-d_2, formaldehyde and their mixtures. *Can. J. Chem*. **42**, 2451–2455 (1964). doi.org/10.1139/v64-360

54. R. D. McQuigg, J. G. Calvert, Photodecomposition of CH_2O, CD_2O, CHDO, and CH_2O-CD_2O mixtures at xenon flash lamp intensities. *J. Am. Chem. Soc.* **91**, 1590-1599 (1969). doi.org/10.1021/ja01035a002

55. H. P. Sperling, S. Toby, The photochemical decomposition of gaseous formaldehyde. *Can. J. Chem*. **51**, 471–475 (1973). doi.org/10.1139/v73-072

56. P. Morajkar, A. Bossolasco, C. Schoemaecker, C. Fittschen, Photolysis of CH_3CHO at 248 nm: Evidence of triple fragmentation from primary quantum yield of CH_3 and HCO radicals and H atoms. *J. Chem. Phys.* **140**, 214308 (2014). doi.org/10.1063/1.4878668

57. A. B. Guenther, X. Jiang, C. L. Heald, T. Sakulyanontvittaya, T. Duhl, L. K. Emmons, X. Wang, The model of emissions of gases and aerosols from nature version 2.1 (MEGAN2.1): An extended and updated framework for modeling biogenic emissions. *Geosci. Model Dev*. **5**, 1471–1492 (2012). doi.org/10.5194/gmd-5-1471-2012

58. P. O. Wennberg, K. H. Bates, J. D. Crounse, L. G. Dodson, R. C. McVay, L. A. Mertens, T. B. Nguyen, E. Praske, R. H. Schwantes, M. D. Smarte, J. M. St Clair, A. P. Teng, X. Zhang, J. H. Seinfeld, Gas-phase reactions of isoprene and its major oxidation products. *Chem Rev*. **118**, 3337–3390 (2018). doi.org/10.1021/acs.chemrev.7b00439

59. M. Staak, E. W. Gash, D. S. Venables, A. A. Ruth, The rotationally-resolved absorption spectrum of formaldehyde from 6547 to 6804 cm^{-1}, *J. Mol. Spectrosc*. **229**, 115–121 (2005). doi.org/10.1016/j.jms.2004.08.019

60. A. A. Ruth, U. Heitmann, E. Heinecke, C. Fittschen, C., The rotationally resolved absorption spectrum of formaldehyde from 6547 to 7051 cm^{-1}, *Z. Phys. Chem*. **229**, 1609–1624 (2015). doi.org/10.1515/zpch-2015-0623

61. Gaussian 16, Revision C.01, M. J. Frisch, G. W. Trucks, H. B. Schlegel, G. E. Scuseria, M. A. Robb, J. R. Cheeseman, G. Scalmani, V. Barone, G. A. Petersson, H. Nakatsuji, X. Li, M. Caricato, A. V. Marenich, J. Bloino, B. G. Janesko, R. Gomperts, B. Mennucci, H. P. Hratchian, J. V. Ortiz, A. F. Izmaylov, J. L. Sonnenberg, D. Williams-Young, F. Ding, F. Lipparini, F. Egidi, J. Goings, B. Peng, A. Petrone, T. Henderson, D. Ranasinghe, V. G. Zakrzewski, J. Gao, N. Rega, G. Zheng, W. Liang, M. Hada, M. Ehara, K. Toyota, R. Fukuda, J. Hasegawa, M. Ishida, T. Nakajima, Y. Honda, O. Kitao, H. Nakai, T. Vreven, K. Throssell, J. A. Montgomery, Jr., J. E. Peralta, F. Ogliaro, M. J. Bearpark, J. J. Heyd, E. N. Brothers, K. N. Kudin, V. N. Staroverov, T. A. Keith, R. Kobayashi, J. Normand, K. Raghavachari, A. P. Rendell, J. C. Burant, S. S. Iyengar, J. Tomasi, M. Cossi, J. M. Millam, M. Klene, C. Adamo, R. Cammi, J. W. Ochterski, R. L. Martin, K. Morokuma, O. Farkas, J. B. Foresman, and D. J. Fox, Gaussian, Inc., Wallingford CT, 2016.

62. D. G. Truhlar, R. Steckler, and M. S. Gordon, Potential energy surfaces for polyatomic reaction dynamics, *Chem. Rev*. **87**, 217–236 (1987). doi.org/10.1021/cr00077a011

63. J. L. Durant, Evaluation of transition state properties by density functional theory, *Chem. Phys. Lett*. **256**, 595–602 (1996). doi.org/10.1016/0009-2614(96)00478-2

64. M. F. Shaw, Photochemical Formation of Enols from Carbonyls. (Ph.D. Thesis, The University of Sydney, 2017).

65. K. N. H. Rowell, S. H. Kable, M. J. T. Jordan, An assessment of the tropospherically accessible photo-initiated ground state chemistry of organic carbonyls *Atmos. Chem. Phys.* **2022**, 929–949 (2022). doi.org/10.5194/acp-22-929-2022

66. M. L. Laury, S. E Boesch, I. Haken, P. Sinha, M. J. Carlson, A. K. Wilson, Harmonic vibrational frequencies: scale factors for pure, hybrid, hybrid meta, and double-hybrid functionals in conjunction with correlation consistent basis sets. *J. Comp. Chem.* **32**, 2339–2347 (2011). doi.org/10.1002/jcc.21811

67. M. K. Kesharwani, B. Brauer, J. M. L. Martin, Frequency and zero-point vibrational energy scale factors for double-hybrid density functionals (and other selected methods): Can anharmonic force fields be avoided? *J. Phys. Chem. A* **119**, 1701–1714 (2015). doi.org/10.1021/jp508422u

68. NIST Computational Chemistry Comparison and Benchmark Database, NIST Standard Reference Database Number 101 Release 21, August 2020, Editor: R. D. Johnson III http://cccbdb.nist.gov/ accessed 1 March 2021.

69. K. G. Lubic, T. Amano, H. Uehara, K. Kawaguchi, E. Hirota, The ν_1 band of the DO_2 radical by difference frequency laser and diode laser spectroscopy: The equilibrium structure of the hydroperoxyl radical, *J. Chem. Phys*. **81**, 4826–4831 (1984). doi.org/10.1063/1.447508

70. G. Herzberg, Electronic spectra and electronic structure of polyatomic molecules (Van Nostrand Reinhold, New York, 1966).

71. K. P. Huber and G. Herzberg, Molecular Spectra and Molecular Structure IV. Constants of Diatomic Molecules (Van Nostrand Reinhold, New York, 1979).

72. J. L. Duncan, The ground-state average and equilibrium structures of formaldehyde and ethylene, *Mol. Phys.* **28**, 1177–1191 (1974). doi.org/10.1080/00268977400102501

73. K. N. Rowell, S. H. Kable, M. J. T. Jordan, Structural effects on the Norrish Type I α-bond cleavage of tropospherically important carbonyls. *J. Phys. Chem. A*, **123**, 10381−10396 (2019). doi.org/10.1021/acs.jpca.9b05534

74. C. M. Western, PGOPHER, A Program for Simulating Rotational, Vibrational and Electronic Spectra. *J Quant. Spectrosc Rad. Transfer*, **186** 221–242 (2017). doi.org/10.1016/j.jqsrt.2016.04.010

75. R. Atkinson, D. L. Baulch, R. A. Cox, J. N. Crowley, R. F. Hampson, R. G. Hynes, M. E. Jenkin, M. J. Rossi, J. Troe, Evaluated kinetic and photochemical data for atmospheric chemistry: Volume I - gas phase reactions of Ox, HOx, NOx and SOx species. *Atmos. Chem. Phys.*, **4**, 1461–1738 (2004). doi.org/10.5194/acp-4-1461-2004

76. C. A. Smith, F. D. Pope, B. Cronin, C. B. Parkes, and A. J. Orr-Ewing, Absorption cross sections of formaldehyde at wavelengths from 300 to 340 nm and at 294 and 245 K, *J. Phys. Chem. A* **110**, 11645–11653 (2006). doi.org/10.1021/jp063713y

77. K. Chance and J. Orphal, Revised ultraviolet absorption cross sections of HCHO for the HITRAN database, *J. Quant. Spectrosc. Radiat. Transfer* **112**, 1509-1510 (2011). doi.org/10.1016/j.jqsrt.2011.02.

78. S. P. Sander, R. R. Friedl, D. M. Golden, M. J. Kurylo, R. E. Huie, G. K. Moortgat, H. Keller-Rudek, P. H. Wine, A. R. Ravishankara, C. E. Kolb, M. J. Molina, B. J. Finlayson-Pitts, V. L. Orking Orking, Chemical kinetics and photochemical data for use in atmospheric studies NASA JPL Evaluation No. 15JPL Publication 06-2 (2006).

79. D. C. Tardy, B. S. Rabinovitch, Intermolecular vibrational energy transfer in thermal unimolecular systems. *Chem. Rev. 77*, 369-408 (1977). doi.org/10.1021/cr60307a004

80. A. B. Weaver, A. A. Alexeenko, Revised Variable Soft Sphere and Lennard-Jones Model Parameters for Eight Common Gases up to 2200 K. *J. Phys. Chem. Ref. Data* **44**, 023103 (2015). doi.org/10.1063/1.4921245.

81. J. Troe, Mixture Rules in Thermal Unimolecular Reactions. *Ber. Bunsenges. Phys. Chem*. **84**, 829-834, (1980). doi.org/10.1002/bbpc.19800840902

82. J. R. Barker, L. M. Yoder, K. D. King, Vibrational energy transfer modeling of non-equilibrium polyatomic reaction systems. *J. Phys. Chem. A **105***, 796-809 (2001). doi.org/10.1021/jp002077f

83. A. W. Jasper, "Third-body" collision parameters for hydrocarbons, alcohols, and hydroperoxides and an effective internal rotor approach for estimating them. *Int J Chem Kinet.* **52**, 387-402 (2020). doi.org/10.1002/kin.21358

84. S. J. Klippenstein, An efficient procedure for evaluating the number of available states within a variably defined reaction coordinate framework. *J. Phys. Chem.* **98**, 11459-11464 (1994). doi.org/10.1021/j100095a032

85. K. L. K. Lee, M. S. Quinn, S. J. Kolmann, S. H. Kable, M. J. T. Jordan, Zero-point energy conservation in classical trajectory simulations: Application to H_2CO, *J. Chem. Phys*. **148**, 194113 (2018). doi.org/10.1063/1.5023508

86. A. W. Jasper, C. M. Oana, J. A. Miller, "Third-Body" collision efficiencies for combustion modeling: Hydrocarbons in atomic and diatomic baths *Proc. Combust. Inst.* **35**, 197-2040 (2015). doi.org/10.1016/j.proci.2014.05.105

87. A. W. Jasper, J. A. Miller, Theoretical Unimolecular Kinetics for $CH_4 + M \rightleftarrows CH_3 + H + M$ in Eight Baths, M = He, Ne, Ar, Kr, H_2, N_2, CO, and CH_4. *J. Phys. Chem. A* 115, 6438-6455 (2011). doi.org/10.1021/jp200048n